

Many-body large polaron optical conductivity in $\text{SrTi}_{1-x}\text{Nb}_x\text{O}_3$

J. T. Devreese^{1,*}, S. N. Klimin^{1,**}, J. L. M. van Mechelen², and D. van der Marel²

¹*Theorie van Kwantumsystemen en Complexe Systemen, Universiteit Antwerpen, Groenenborgerlaan 171, B-2020 Antwerpen, Belgium and*

²*Département de Physique de la Matière Condensée, Université de Genève, Genève, Switzerland*

(Dated: July 31, 2021)

Recent experimental data on the optical conductivity of niobium doped SrTiO_3 are interpreted in terms of a gas of large polarons with effective coupling constant $\alpha_{eff} \approx 2$. The theoretical approach takes into account many-body effects, the electron-phonon interaction with multiple LO-phonon branches, and the degeneracy and the anisotropy of the Ti t_{2g} conduction band. Based on the Fröhlich interaction, the many-body large-polaron theory provides an interpretation for the essential characteristics, except – interestingly – for the unexpectedly large intensity of a peak at ~ 130 meV, of the observed optical conductivity spectra of $\text{SrTi}_{1-x}\text{Nb}_x\text{O}_3$ *without* any adjustment of material parameters.

I. INTRODUCTION

The infrared optical absorption of perovskite-type materials, in particular, of copper oxide based high- T_c superconductors and of the manganites has been the subject of intensive investigations [3–12]. Insulating SrTiO_3 has a perovskite structure and manifests a metal–insulator transition at room temperature around a doping of 0.002% La or Nb per unit cell [13]. At low doping concentrations, between 0.003% and 3%, strontium titanate reveals a superconducting phase transition [14] below 0.7 K. Various optical experiments [13, 15–19] show a mid-infrared band in the normal state optical conductivity of doped SrTiO_3 which is often explained by polaronic behavior. In the recently observed optical conductivity spectra of Ref. [17], shown in Fig. 1, there is a broad mid-infrared optical conductivity band starting at a photon energy of $\hbar\Omega \sim 100$ meV, which is within the range of the LO-phonon energies of $\text{SrTi}_{1-x}\text{Nb}_x\text{O}_3$. The peaks/shoulders of the experimental optical conductivity band at $\hbar\Omega \sim 200$ to 400 meV resemble the peaks provided by the mixed plasmon-phonon excitations as described in Ref. [20]. Based on the experimental data, the authors deduce a coupling constant $3 < \alpha < 4$ and conclude the mid-infrared peaks to originate from large polaron formation. The high and narrow peaks positioned at the lower frequencies with respect to the mid-infrared band are attributed in Ref. [17] to the optical absorption of the TO-phonons.

There are different types of polaron states in solids. In the effective mass approximation for the electron placed in a continuum polarizable medium, a so-called large or continuum polaron can exist. Large polaron wave functions and the corresponding lattice distortions spread over many lattice sites. Due to the finite phonon frequencies the ion polarizations can follow the polaron motion if the motion is sufficiently slow. Hence, large polarons with a low kinetic energy propagate through the lattice as free electrons but with an enhanced effective mass. When the polaron binding energy is larger than the half bandwidth of the electron band, all states in the Bloch bands are ‘dressed’ by phonons. In this strong-coupling

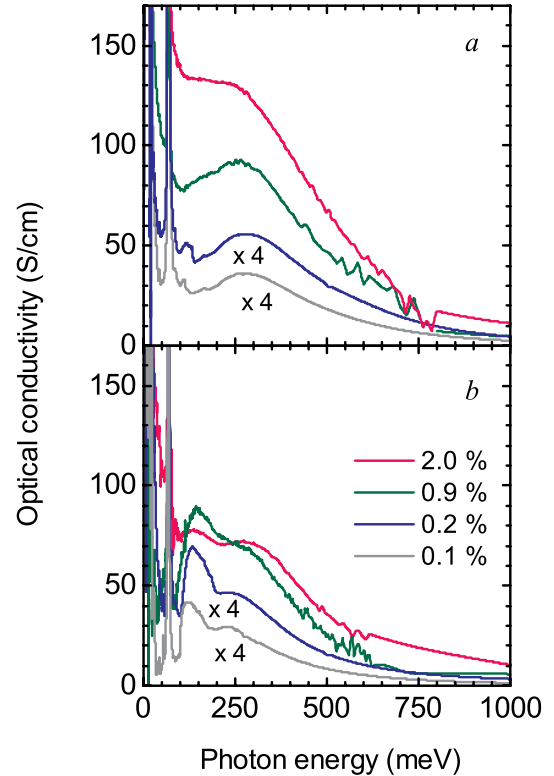


FIG. 1: Optical conductivity of $\text{SrTi}_{1-x}\text{Nb}_x\text{O}_3$ for 0.1% (grey curves), 0.2% (blue curves), 0.9% (green curves) and 2% (pink curves) at 300 K (panel a) and 7 K (panel b). For clarity, the mid-infrared conductivities of $x = 0.1\%$ and 0.2% are magnified by a factor 4. (From Ref. [17].)

regime, the finite electron bandwidth becomes important, so the continuum approximation cannot be applied. In this case the carriers are described as “small” or discrete (lattice) polarons that can hop between different states localized at lattice sites. A key distinction between large and small polarons is then the radius of the polaron state. For large polarons, that radius substantially exceeds the lattice constant, while for small polarons it is comparable to the lattice constant. A review of the properties

of large and small polarons can be found, e. g., in Refs. [21, 22]. In the theory of “mixed” polarons [23–26] the states of the electron-phonon system are composed of a mixture of large and small polaron states.

Polaron states are formed due to the electron-phonon interaction, which is different in the cases of large and small polarons. For a large polaron, the electron-phonon interaction is provided by a macroscopic (continuum) polarization of the lattice. This interaction is characterized by the coupling constant α introduced by Fröhlich [27],

$$\alpha = \frac{1}{2} \left(\frac{1}{\varepsilon_\infty} - \frac{1}{\varepsilon_0} \right) \frac{e^2}{\hbar\omega_L} \left(\frac{2m_b\omega_L}{\hbar} \right)^{1/2}, \quad (1)$$

where ε_∞ and ε_0 are, respectively, the high-frequency and the static dielectric constants, e is the electron charge, ω_L is the longitudinal optical (LO) phonon frequency in the Brillouin zone centre, and m_b is the band electron (or hole) mass. The large-polaron coupling constant is thus expressed through macroscopic observable parameters of a polarizable medium. On the contrary, the electron-phonon interaction for a small polaron is described through microscopic parameters.

The nature of the polaron states in $\text{SrTi}_{1-x}\text{Nb}_x\text{O}_3$ is not yet clear. Previous optical measurements on strontium titanate were interpreted in terms of small polarons [26, 28]. However, that assumption contradicts the interpretation of transport measurements [29], which rather support the large-polaron picture. Also the heat capacity measurements [30], provide effective masses similar to those of large polarons. In Ref. [15], the experimental results of Ref. [18] on the temperature-dependent plasma frequencies in $\text{SrTi}_{1-x}\text{Nb}_x\text{O}_3$ were interpreted within the theory of mixed polarons [23–26]. Thermoelectric power measurements [29] have shown that the density-of-states masses increase with increasing temperature, which can be explained by a theory of mixed polarons [23]. It has been supposed [16] that the polaron optical conductivity in $\text{SrTi}_{1-x}\text{Nb}_x\text{O}_3$ is probably provided by mixed polarons. A possible coexistence of large and small mass polarons has been suggested in Ref. [31]. In Ref. [32], coexistence of small and large polarons in the same solid is invoked to interpret experimental data on the optical absorption in oxides.

The key question is to determine the type of polarons that provide the mechanism of the polaron optical conductivity in $\text{SrTi}_{1-x}\text{Nb}_x\text{O}_3$. The optical response of large polarons in various approximations was studied, e. g., in Refs. [33–36]. The same problem for the small polaron was investigated in [28, 37]. In the large-polaron theory, the optical absorption is provided by transitions (with 0, 1, . . . phonon emission) between different continuum electron states. In the small-polaron theory, the optical absorption occurs when the self-trapped carrier is induced to transfer from its localized state to a localized state at an adjacent site, with emission of phonons. Because of the different physical mechanisms involved, the optical conductivity spectra of large and small polarons are different from each other. In the large-polaron

theory the polaron optical conductivity behaves at high frequencies Ω as a power function ($\propto \Omega^{-5/2}$). In the small-polaron theory, the polaron optical conductivity at high frequencies decreases much faster than for large polarons: as a Gaussian exponent. Therefore the analysis of optical measurements can shed some light on the afore-said question on the type of polarons responsible for the optical conductivity in $\text{SrTi}_{1-x}\text{Nb}_x\text{O}_3$.

The polaron optical conductivity band of $\text{SrTi}_{1-x}\text{Nb}_x\text{O}_3$ occupies the mid-infrared range of the photon energies $\hbar\Omega \lesssim 1$ eV, and the threshold for interband electron-hole transitions lies at the band gap energy, which is around 3.3 eV in $\text{SrTi}_{1-x}\text{Nb}_x\text{O}_3$ [17]. Therefore interband transitions do not interfere with the polaron optical conductivity. Other mechanisms of electron intraband scattering (for example, electron-phonon interaction with acoustic phonons and/or electron or hole transitions from impurity centers) may be manifested together with the polaron mechanism in the energy range $\hbar\Omega \lesssim 1$ eV. The treatment of those mechanisms is, however, beyond the scope of the present investigation.

We can make some preliminary suggestions concerning the dominating mechanism of the mid-infrared optical conductivity in the Nb doped strontium titanate. The low-frequency edge of the mid-infrared band in $\text{SrTi}_{1-x}\text{Nb}_x\text{O}_3$ at a low temperature ($T = 7$ K) lies in the range of the LO-phonon energies obtained in [18]. The maximum of the mid-infrared band lies relatively close to this low-frequency edge (the difference in frequency between the low-frequency edge and the maximum of the mid-infrared band is comparable to the LO-phonon frequencies in $\text{SrTi}_{1-x}\text{Nb}_x\text{O}_3$). This behavior is characteristic of large-polaron optical conductivity rather than of small-polaron optical conductivity. Indeed, the maximum of the small polaron optical conductivity band is expected to be shifted to considerably higher frequencies with respect to the low-frequency edge of the polaron optical conductivity band (see, e.g., Ref. [37]). Also, at sufficiently high frequencies, the experimental mid-infrared band from Ref. [17] decreases with increasing Ω rather slowly, which is characteristic for large-polaron optical conductivity rather than for small-polaron optical conductivity. We therefore can suggest that the large-polaron picture is the most appropriate for the interpretation of the mid-infrared band of $\text{SrTi}_{1-x}\text{Nb}_x\text{O}_3$ observed in Ref. [17].

In order to interpret the mid-infrared band of the experimental optical conductivity spectra of $\text{SrTi}_{1-x}\text{Nb}_x\text{O}_3$ [17] in terms of polarons, we calculate the large-polaron optical conductivity spectra for $\text{SrTi}_{1-x}\text{Nb}_x\text{O}_3$ using the model for the optical conductivity of a large-polaron gas developed in Ref. [20], adapted to take into account multiple LO-phonon branches [38]. The degeneracy and the anisotropy of the conduction band in $\text{SrTi}_{1-x}\text{Nb}_x\text{O}_3$ are taken into account.

The paper is organized as follows. In Sec. II we describe the theoretical formalism for the polaron optical

conductivity. In Sec. III the calculated polaron optical conductivity spectra are discussed and compared with the experiment [17]. Sec. IV contains conclusions.

II. OPTICAL CONDUCTIVITY OF A GAS OF LARGE POLARONS

The optical absorption spectra of $\text{SrTi}_{1-x}\text{Nb}_x\text{O}_3$ are sensitive to the doping level [17]. Therefore a many-polaron description is in order. In our context, “many-polaron description” means an account of many-electron effects on the optical conductivity of a polaron gas. These effects include the influence of the electron-electron Coulomb interaction (which leads to screening effects) and of the Fermi statistics of the polaron gas on the optical conductivity spectra. In the low-density limit, those many-body effects are not important, and the optical conductivity of a polaron gas is well described by the optical conductivity of a single polaron multiplied by the electron density. The scope of the present study embraces a wide range of electron densities for which the single-polaron approach is, in general, insufficient. As shown below, even at the lowest electron density involved in the experiment [17], the shape and magnitude of the optical conductivity spectrum is strongly affected by many-body effects.

We wish to compare the experiments of Ref. [17], in particular the observed mid-infrared band, to the theoretical optical conductivity of a gas of large polarons. For that purpose we use the many-body large polaron approach of Refs. [20, 38], which takes into account the electron-electron interaction and the Fermi statistics of polarons.

Refs. [20, 38] are limited to the study of weak-coupling polarons. Up to $\alpha \approx 3$, which includes the case of $\text{SrTi}_{1-x}\text{Nb}_x\text{O}_3$, the weak coupling approximation can be expected to describe the main characteristics of the many-polaron optical response (see, e.g., Refs. [20–22]). In Ref. [38] a generalization of Ref. [20] is presented that takes into account the electron-phonon interaction with *multiple LO-phonon branches* as they exist, e. g., in complex oxides. For a single polaron, effects related to multiple LO-phonon branches were investigated in Ref. [40]. The starting point for the treatment of a many-polaron system is the Fröhlich Hamiltonian

$$H = \sum_{\mathbf{k}} \sum_{\sigma=\pm 1/2} \frac{\hbar^2 k^2}{2m_b} c_{\mathbf{k},\sigma}^+ c_{\mathbf{k},\sigma} + \sum_{\mathbf{q}} \sum_{j=1}^n \hbar\omega_{L,j} a_{\mathbf{q},j}^+ a_{\mathbf{q},j} + U_{e-e} + \frac{1}{\sqrt{V}} \sum_{\mathbf{q}} \sum_{j=1}^n \left(V_{\mathbf{q},j} a_{\mathbf{q},j} \sum_{\mathbf{k}} \sum_{\sigma=\pm 1/2} c_{\mathbf{k}+\mathbf{q},\sigma}^+ c_{\mathbf{k},\sigma} + \text{h.c.} \right), \quad (2)$$

where $c_{\mathbf{k},\sigma}^+$ ($c_{\mathbf{k},\sigma}$) are the creation (annihilation) operators for an electron with momentum \mathbf{k} and with the spin z -projection σ , $a_{\mathbf{q},j}^+$ ($a_{\mathbf{q},j}$) are the creation (annihilation)

operators for a phonon of the j -th branch with the momentum q , $\omega_{L,j}$ are the LO-phonon frequencies (approximated here as non-dispersive), and V is the volume of the crystal. The polaron interaction amplitude $V_{\mathbf{q},j}$ is [40]

$$V_{\mathbf{q},j} = \frac{\hbar\omega_{L,j}}{q} \left(\frac{4\pi\alpha_j}{V} \right)^{1/2} \left(\frac{\hbar}{2m_b\omega_{L,j}} \right)^{1/4}, \quad (3)$$

where α_j is a dimensionless partial coupling constant characterizing the interaction between an electron and the j -th LO-phonon branch. The electron-electron interaction is described by the Coulomb potential energy

$$U_{e-e} = \frac{1}{2} \sum_{\mathbf{q} \neq 0} \frac{4\pi e^2}{\varepsilon_\infty q^2} \sum_{\mathbf{k}, \mathbf{k}', \sigma, \sigma'} c_{\mathbf{k}+\mathbf{q},\sigma}^+ c_{\mathbf{k}'-\mathbf{q},\sigma'}^+ c_{\mathbf{k}',\sigma'} c_{\mathbf{k},\sigma}. \quad (4)$$

Optical phonons in SrTiO_3 show a considerable dispersion (see, e. g., Ref. [41] and references therein). The effect of the phonon dispersion is a broadening of features of the polaron optical conductivity band. The magnitude of the broadening is characterized by the dispersion parameter $\Delta\omega$ of the optical phonons, that contribute to the integrals over \mathbf{q} entering the polaron optical conductivity. In a polar crystal with a single LO-phonon branch, that range of convergence is approximately $q_0 = (m_b\omega_{LO}/\hbar)^{1/2}$. For SrTiO_3 , taking $\omega_{LO} = \max\{\omega_{L,j}\}$, we obtain $q_0 \approx 1.02 \times 10^9 \text{ m}^{-1}$. The boundary of the Brillouin zone π/a_0 in SrTiO_3 (where the lattice constant $a_0 \approx 0.3905 \text{ nm}$) is at $8 \times 10^9 \text{ m}^{-1}$. Therefore the integration domain for the relevant integrals is one order smaller than the size of the Brillouin zone. In the region $0 < q < q_0$, the dispersion parameter of the LO-phonon frequencies, $\Delta\omega$, is a few percent of $\omega_{L,j}$. Consequently, $\Delta\omega$ is very small compared with the characteristic width of the polaron band. Therefore, in the present treatment, we apply the approximation of non-dispersive phonons.

For a description of a polarizable medium with n optical-phonon branches, we use the model dielectric function [42, 43]

$$\varepsilon(\omega) = \varepsilon_\infty \prod_{j=1}^n \left(\frac{\omega^2 - \omega_{L,j}^2}{\omega^2 - \omega_{T,j}^2} \right), \quad (5)$$

whose zeros (poles) correspond to the LO(TO) phonon frequencies $\omega_{L,j}$ ($\omega_{T,j}$). This dielectric function is the result of the straightforward extension of the Born-Huang approach [44] to the case where more than one optical-phonon branch exists in a polar crystal. The Born-Huang approach and its extension [42] generate expressions for the macroscopic polarization induced by the polar vibrations, and for the corresponding electrostatic potential. This electrostatic potential is a basis element of the Hamiltonian of the electron-phonon interaction. In Ref. [42], the Hamiltonian of the electron-phonon interaction

has been explicitly derived with the amplitudes

$$V_{\mathbf{q}j} = \frac{1}{\sqrt{V}} \frac{e}{iq} \left(\frac{4\pi\hbar}{\left. \frac{\partial \varepsilon(\omega)}{\partial \omega} \right|_{\omega=\omega_{L,j}}} \right)^{1/2}. \quad (6)$$

Using Eqs. (3) and (6) with the dielectric function (5), we arrive at the following set of linear equations for the coupling constants α_j ($j = 1, \dots, n$):

$$\sum_{k=1}^n \hbar \omega_{L,k}^3 \left(\frac{\hbar}{2m_b \omega_{L,k}} \right)^{1/2} \frac{\alpha_k}{\omega_{L,k}^2 - \omega_{T,j}^2} = \frac{e^2}{2\varepsilon_\infty}. \quad (7)$$

Knowledge of the band mass, of the electronic dielectric constant ε_∞ and of the LO- and TO-phonon frequencies is sufficient to determine the coupling constants α_j taking into account mixing between different optical-phonon branches. In the particular case of a single LO-phonon branch, Eq. (7) is reduced to (1).

In order to describe the optical conductivity of a polaron gas, we refer to the work [46], where the Mori-Zwanzig projection operator technique has been used to rederive the path-integral result of Ref. [45] and the impedance of Ref. [33]. We repeat the derivations of Ref. [46] with the replacement of single-electron functions by their many-electron analogs. For example, $e^{i\mathbf{q}\cdot\mathbf{r}}$ in the Hamiltonian of the electron-phonon interaction is replaced by the Fourier component of the electron density for an N -electron system,

$$\rho(\mathbf{q}) \equiv \sum_{s=1}^N e^{i\mathbf{q}\cdot\mathbf{r}_s} = \sum_{\mathbf{k},\sigma} c_{\mathbf{k}+\mathbf{q},\sigma}^\dagger c_{\mathbf{k},\sigma}. \quad (8)$$

As a result, we arrive at a formula which is structurally similar to the single-polaron optical conductivity [33, 46],

$$\sigma(\Omega) = \frac{e^2 n_0}{m_b} \frac{i}{\Omega - \chi(\Omega)/\Omega}, \quad (9)$$

where $n_0 = N/V$ is the carrier density, and $\chi(\Omega)$ is the memory function. The same many-electron derivation as in the present work, to the best of our knowledge, was first performed for the polaron gas in 2D in Ref. [47] in the weak electron-phonon coupling limit.

In Refs. [33, 46] the single-polaron memory function was calculated starting from the all-coupling Feynman variational principle [48]. For a many-polaron system, an effective all-coupling extension of that variational principle has not been worked out yet. In the present treatment, we restrict ourselves to the weak-coupling approximation for the electron-phonon interaction to derive the memory function. In this approximation, the memory function $\chi(\Omega)$ is similar to that of Ref. [47], with two distinctions: (1) the electron gas in the present treatment is three-dimensional, (2) several LO phonon branches are taken into account. The resulting form of the memory

function is

$$\chi(\Omega) = \frac{4}{3\hbar m_b n_0 V} \sum_{\mathbf{q},j} q^2 |V_{\mathbf{q},j}|^2 \int_0^\infty dt (e^{i\Omega t} - 1) \times \text{Im} \left[\frac{\cos[\omega_{L,j}(t + i\hbar\beta/2)]}{\sinh(\beta\hbar\omega_{L,j}/2)} S(\mathbf{q}, t) \right], \quad (10)$$

where $\beta = 1/(k_B T)$. The dynamical structure factor $S(\mathbf{q}, t)$ is proportional to the two-point correlation function (cf. Ref. [20]),

$$S(\mathbf{q}, t) \equiv \frac{1}{2} \left\langle \sum_{i,j=1}^N e^{i\mathbf{q}\cdot[\mathbf{r}_j(t) - \mathbf{r}_i(0)]} \right\rangle = \frac{1}{2} \langle \rho(\mathbf{q}, t) \rho(-\mathbf{q}, 0) \rangle. \quad (11)$$

To obtain $\chi(\Omega)$ to order α it is sufficient to perform the averaging in the correlation function (11) using the Hamiltonian (2) without the electron-phonon interaction and keeping the electron-electron interaction term U_{e-e} .

We calculate the dynamical structure factor (11) extending the method [20] to nonzero temperatures. In Ref. [20], the key advantage of the many-polaron variational approach [49] is exploited: the fact that the many-body effects are entirely contained in the dynamical structure factor $S(\mathbf{q}, t)$. The structure factor can be calculated using various approximations. Terms of order of $|V_{\mathbf{q},j}|^2$ are automatically taken into account in the memory function (10). Consequently, up to order α for $\sigma(\Omega)$, it is sufficient to calculate $S(\mathbf{q}, t)$ without the electron-phonon coupling. In Ref. [20], $S(\mathbf{q}, t)$ was calculated within two different approximations: (i) the Hartree-Fock approximation, (ii) the random-phase approximation (RPA). As shown in Ref. [20], the RPA dynamical structure factor, contrary to the Hartree-Fock approximation, takes into account the effects both of the Fermi statistics and of the electron-electron interaction on the many-polaron optical-absorption spectra.

The dynamical structure factor is expressed through the density-density Green's functions defined as

$$\mathcal{G}(\mathbf{q}, \Omega) \equiv -i \int_0^\infty e^{i\Omega t} \langle \rho(\mathbf{q}, t) \rho(-\mathbf{q}, 0) \rangle dt, \quad (12)$$

$$G^R(\mathbf{q}, \Omega) \equiv -i \int_0^\infty e^{i\Omega t} \langle [\rho(\mathbf{q}, t), \rho(-\mathbf{q}, 0)] \rangle dt. \quad (13)$$

In terms of $G(\mathbf{q}, \Omega)$ and $G^R(\mathbf{q}, \Omega)$, the memory function (10) takes the form:

$$\chi(\Omega) = \sum_j \frac{\alpha_j \hbar \omega_{L,j}^2}{6\pi^2 N m_b} \left(\frac{\hbar}{2m_b \omega_{L,j}} \right)^{1/2} \times \int d\mathbf{q} \{ \mathcal{G}(\mathbf{q}, \Omega - \omega_{L,j}) + \mathcal{G}^*(\mathbf{q}, -\Omega - \omega_{L,j}) - \mathcal{G}(\mathbf{q}, -\omega_{L,j}) - \frac{1}{e^{\beta\hbar\omega_{L,j}} - 1} [G^R(\mathbf{q}, \Omega - \omega_{L,j}) + (G^R(\mathbf{q}, -\Omega - \omega_{L,j}))^* - G^R(\mathbf{q}, -\omega_{L,j}) - (G^R(\mathbf{q}, -\omega_{L,j}))^*] \}. \quad (14)$$

Taking into account the Coulomb electron-electron interaction within RPA, the retarded Green's function

$G^R(\mathbf{q}, \Omega)$ is given by

$$G^R(\mathbf{q}, \Omega) = \frac{\hbar V P^{(1)}(\mathbf{q}, \Omega)}{1 - \frac{4\pi e^2}{\varepsilon_\infty q^2} P^{(1)}(\mathbf{q}, \Omega)}, \quad (15)$$

where $P^{(1)}(\mathbf{q}, \Omega)$ is the polarization function of the free electron gas, see, e.g., [50]

$$P^{(1)}(\mathbf{q}, \Omega) = \frac{1}{V} \sum_{\mathbf{k}, \sigma} \frac{f_{\mathbf{k}+\mathbf{q}, \sigma} - f_{\mathbf{k}, \sigma}}{\hbar\Omega + \frac{\hbar^2(\mathbf{k}+\mathbf{q})^2}{2m_b} - \frac{\hbar^2 k^2}{2m_b} + i\delta}, \quad \delta \rightarrow +0 \quad (16)$$

with the electron average occupation numbers $f_{\mathbf{k}, \sigma}$. The function $\mathcal{G}(\mathbf{q}, \Omega)$ is obtained from $G^R(\mathbf{q}, \Omega)$ using the exact analytical relation

$$(1 - e^{-\beta\hbar\Omega}) \text{Im} \mathcal{G}(\mathbf{q}, \Omega) = \text{Im} G^R(\mathbf{q}, \Omega) \quad (17)$$

and the Kramers-Kronig dispersion relations for $\mathcal{G}(\mathbf{q}, \Omega)$.

The above expressions are written for an isotropic conduction band. However, the conduction band of $\text{SrTi}_{1-x}\text{Nb}_x\text{O}_3$ is strongly anisotropic and triply degenerate. The electrons are doped in three bands: d_{xy} , d_{yz} and d_{xz} , which all have their minima at $\mathbf{k} = 0$. Each of these bands has light masses along two direction (x and y for d_{xy} , etc.) and a heavy mass along the third direction. While each electron has a strongly anisotropic mass, the electronic transport remains isotropic due to the fact that 2 light masses and 1 heavy mass contribute along each crystallographic axis.

The anisotropy of the electronic effective mass of the conduction band can be approximately taken into account in the following way. We use the averaged inverse band mass

$$\frac{1}{\bar{m}_b} = \frac{1}{3} \left(\frac{1}{m_x} + \frac{1}{m_y} + \frac{1}{m_z} \right) \quad (18)$$

and the density-of-states band mass

$$m_D = (m_x m_y m_z)^{1/3}. \quad (19)$$

The mass m_D appears in the prefactor of the linear term of the specific heat. Comparing the mass m_D obtained from the experimental specific heat [30, 51] with the mass \bar{m}_b obtained using optical spectral weights [17] reveals the mass ratio of the heavy and light bands to be about 27. The expression (18) replaces the bare mass m_b in the optical conductivity (9) and in the memory function (14). The polarization function of the free electron gas (16) is calculated with the density-of-states mass m_D instead of m_b . The band degeneracy is taken into account through the degeneracy factor which is equal to 3, both in the polarization function and in the normalization equation for the chemical potential. The reduction of the polaron optical conductivity band due to screening with band degeneracy turns out to be less significant than without band degeneracy.

III. THEORY AND EXPERIMENT

A. Material parameters

Several experimental parameters characterizing $\text{SrTi}_{1-x}\text{Nb}_x\text{O}_3$ are necessary for the calculation of the large-polaron optical conductivity (see, e.g., Refs. [16, 18]): the LO- and TO-phonon frequencies, the electron band mass, and the electronic dielectric constant ε_∞ .

The electronic dielectric constant can be obtained using reflectivity spectra of $\text{SrTi}_{1-x}\text{Nb}_x\text{O}_3$. At $T = 10$ K, the reflectivity of $\text{SrTi}_{1-x}\text{Nb}_x\text{O}_3$ is $R \approx 0.16$ for $\Omega \approx 5000 \text{ cm}^{-1}$. The electronic dielectric constant can be approximated using the expression

$$R(\Omega) = \left| \frac{\sqrt{\varepsilon(\Omega)} - 1}{\sqrt{\varepsilon(\Omega)} + 1} \right|^2 \quad (20)$$

and assuming that $\Omega = 5000 \text{ cm}^{-1}$ is a sufficiently high frequency to characterize the electronic response. From (20) it follows that for $\text{SrTi}_{1-x}\text{Nb}_x\text{O}_3$, $\varepsilon_\infty \approx 5.44$.

In order to determine the optical-phonon frequencies, we use the experimental data from available sources [17, 18]. In Ref. [17], three infrared active phonon modes are observed at room temperature: at 11.0 meV, 21.8 meV and 67.6 meV. With decreasing temperature, the lowest-frequency infrared-active phonon mode shows a strong red shift upon cooling, and saturates at about 2.3 meV at 7 K. Those infrared-active phonon modes are associated with the polar TO-phonons. The TO-phonon frequencies determined in Ref. [18] for $\text{SrTi}_{1-x}\text{Nb}_x\text{O}_3$ with $x = 0.9\%$ at $T = 300$ K are 100 cm^{-1} , 175 cm^{-1} and 550 cm^{-1} . The corresponding TO-phonon energies are 12.4 meV, 21.7 meV and 68.2 meV.

Refs. [17] and [18] are used as sources for phonon parameters. In Ref. [18], the TO-phonon frequencies are calculated on the basis of reflectivity measurements using a model dielectric function to fit experimental data. In Ref. [17], the TO-phonon frequencies are obtained from an analysis of both reflectivity and transmission spectra, using inversion of the Fresnel equations of reflection and transmission coefficients and the Kramers-Kronig transformation of the reflectivity spectra. The TO-phonon energies reported in Refs. [17] and [18] are in close agreement. This confirms the reliability of both experimental data sources [17, 18]. The values of the TO-phonon frequencies used in our calculation are taken from the experiment [17] because they are directly related to the samples of $\text{SrTi}_{1-x}\text{Nb}_x\text{O}_3$ for which the comparison of theory and experiment is made in the present work.

The TO phonon frequencies from Ref. [17] can be used when they are complemented with corresponding LO phonon frequencies. However, Ref. [17] does not contain data of the LO-phonon frequencies. In the present calculation we use the LO phonon frequencies from Ref. [18].

The averaged band mass (18) is taken to be $\bar{m}_b = 0.81m_e$ (where m_e is the electron mass in vacuum) ac-

TABLE I: Optical-phonon frequencies and partial coupling constants of doped strontium titanate

x	$x = 0.1\%$	$x = 0.1\%$	$x = 0.2\%$	$x = 0.2\%$	$x = 0.9\%$	$x = 0.9\%$	$x = 2\%$	$x = 2\%$
T	$T = 7$ K	$T = 300$ K	$T = 7$ K	$T = 300$ K	$T = 7$ K	$T = 300$ K	$T = 7$ K	$T = 300$ K
$\hbar\omega_{T,1}$ (meV)	2.27	11.5	2.63	11.5	6.01	12.1	8.51	13.0
$\hbar\omega_{L,1}$ (meV)	21.2	21.2	21.2	21.2	21.2	21.2	21.2	21.2
α_1	0.021	0.013	0.021	0.013	0.017	0.013	0.017	0.013
$\hbar\omega_{T,2}$ (meV)	21.2	21.8	21.2	21.8	21.2	21.8	21.2	21.8
$\hbar\omega_{L,2}$ (meV)	58.4	58.4	58.4	58.4	58.4	58.4	58.4	58.4
α_2	0.457	0.414	0.457	0.414	0.452	0.414	0.447	0.409
$\hbar\omega_{T,3}$ (meV)	67.6	67.1	67.6	67.1	67.6	67.1	67.6	67.1
$\hbar\omega_{L,3}$ (meV)	98.7	98.7	98.7	98.7	98.7	98.7	98.7	98.7
α_3	1.582	1.582	1.582	1.580	1.576	1.578	1.570	1.574
α_{eff}	2.06	2.01	2.06	2.01	2.05	2.01	2.03	2.01

ording to experimental data from Ref. [52]. Using the ratio of the heavy mass (m_z) to the light mass ($m_x = m_y$), $m_z/m_x = 27$, we find the density-of-states band mass $m_D \approx 1.65m_e$.

The TO- and LO- phonon frequencies and the resulting partial coupling constants calculated using the mass \bar{m}_b are presented in Table 1.

The effective coupling constant in Table 1 is determined following Ref. [40], as a sum of partial coupling constants α_j ,

$$\alpha_{\text{eff}} \equiv \sum_j \alpha_j \quad (21)$$

The result $\alpha_{\text{eff}} \sim 2$ shows that the electron-phonon coupling strength in $\text{SrTi}_{1-x}\text{Nb}_x\text{O}_3$ lies in the intermediate to weak coupling range, and the conditions for small polaron formation are not fulfilled. This analysis indicates that the large-polaron picture – rather than the small-polaron description is suitable for the interpretation of the mid-infrared band of the optical conductivity of $\text{SrTi}_{1-x}\text{Nb}_x\text{O}_3$.

We use the actual electron densities for the samples studied in Ref. [17] based on the unit cell volume (59.5 cubic angstrom) and the chemical composition (x is the doping level). These carrier densities (see Table 2) are confirmed by measurements of the Hall constants.

TABLE II: Electron densities of $\text{SrTi}_{1-x}\text{Nb}_x\text{O}_3$

x (%)	n_0 (cm^{-3})
0.1	1.7×10^{19}
0.2	3.4×10^{19}
0.9	1.5×10^{20}
2.0	3.4×10^{20}

B. Optical conductivity spectra

We calculate the large-polaron optical conductivity spectra for $\text{SrTi}_{1-x}\text{Nb}_x\text{O}_3$ using the approach of Ref. [20] as adapted in Ref. [38] to take into account multiple LO-phonon branches. We also include in the numerical calculation the TO-phonon contribution to the optical conductivity, described by an oscillatory-like model dielectric function (see, e.g., Ref. [18]):

$$\text{Re } \sigma_{TO}(\Omega) = \sum_j \sigma_{0,j} \frac{\gamma_j^2}{(\Omega - \omega_{T,j})^2 + \gamma_j^2}, \quad (22)$$

where the weight coefficients $\sigma_{0,j}$ and the damping parameters γ_j for each j -th TO-phonon branch are extracted from the experimental optical conductivity spectra of Ref. [17]. The polaron- and the TO-phonon optical responses are treated as independent of each other. Consequently the polaron-(9) and TO-phonon (22) contributions enter the optical conductivity additively.

Following the procedure described above using the material parameters discussed above, we obtain the theoretical large-polaron optical conductivity spectra of $\text{SrTi}_{1-x}\text{Nb}_x\text{O}_3$ shown in Fig. 2 and Fig. 3 at 7 K and 300 K, respectively. In each graph also the experimental optical conductivity spectra of Ref. [17] are shown. It should be emphasized that *in the present calculation, there is no fitting of material constants for the polaron contribution to $\text{Re } \sigma(\Omega)$. Even the magnitude of the optical conductivity, which is often arbitrarily scaled in the literature, follows from first principles.*

At 7 K, the calculated optical conductivity based on the Fröhlich model and extended for a gas of large polarons as described in the present paper, shows convincing agreement with the behavior of the experimental optical conductivity for the high energy part of the spectra, i.e., $\hbar\Omega \gtrsim 300$ meV. The experimental polaron optical conductivity of $\text{SrTi}_{1-x}\text{Nb}_x\text{O}_3$ falls down at high frequencies following the power law (derived in the present work and typical for large polarons) rather than as a

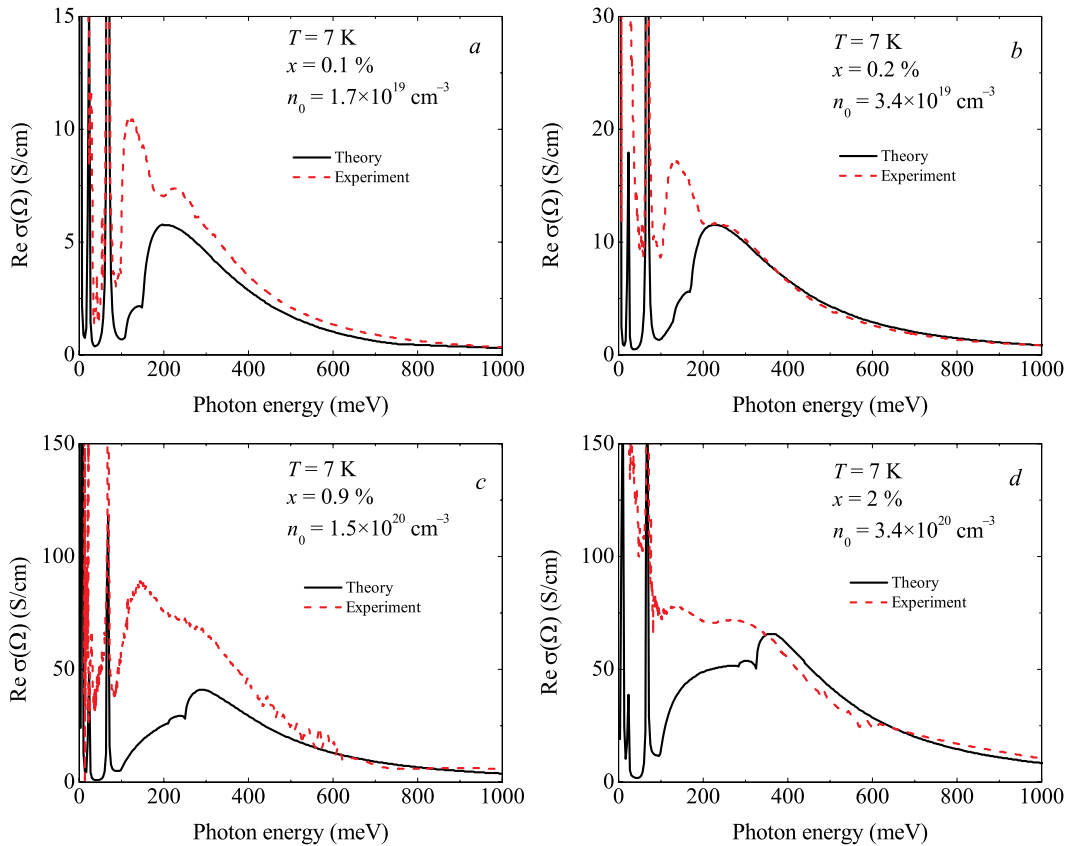


FIG. 2: The many-large-polaron optical conductivity compared with the experiment [17] at $T = 7$ K. The doping level is $x = 0.1\%$ (a), 0.2% (b), 0.9% (c) and 2% (d).

Gaussian exponent that would follow from the small-polaron theory. At lower photon energies $\hbar\Omega \lesssim 200$ meV, the experiment shows distinct peaks that are not explained within the polaron theory. They can be due to other scattering mechanisms as discussed below.

The minor deviations between theoretical and experimental $\text{Re}\sigma(\Omega)$ in the frequency range $\hbar\Omega \gtrsim 300$ meV may be attributed to the difference between the actual electron densities and the densities calculated on the basis of the unit cell volume and the chemical composition. However, we prefer not to fit of the density.

The optical conductivity calculated for a single large-polaron absorption [33] predicts an intensity 3-4 times larger than the experimental data for the lowest doping level $x = 0.1\%$, and therefore cannot explain those data. For higher dopings, the overestimation of the magnitude of the optical conductivity within the single-polaron theory is even larger than for $x = 0.1\%$. Therefore the many-polaron approach, used in the present work, is essential.

At 300 K, in Fig. 3 (a, b, d), the agreement between theory and experiment is qualitative. Both experimental and theoretical spectra show a maximum at the room-temperature optical conductivity spectra in the range $\hbar\Omega \sim 250$ meV. For the doping level $x = 0.9\%$ the calculated optical conductivity spectrum underestimates the

experimental data, as also observed at 7 K.

Many-body effects considerably influence the optical conductivity spectra of a polaron gas. First, features related to the emission of a plasmon together with a LO phonon [20] are manifested in the optical conductivity spectra of the many-polaron gas at $T = 7$ K as separate peaks whose positions shift to higher energies with increasing doping level. At room temperature, those peaks are strongly broadened and smoothed, and only a broad plasmon feature is apparent. Second, the mid-infrared optical conductivity (per particle) in $\text{SrTi}_{1-x}\text{Nb}_x\text{O}_3$ is decreasing at higher doping levels due to the screening of the polar interactions, which is accounted for in the present approach in which $S(\mathbf{q}, t)$ is based on RPA. The effect of screening can be illustrated by the fact that for $n_0 \sim 10^{20} \text{ cm}^{-3}$, the many-polaron optical conductivity *per particle* is reduced by about an order of magnitude compared to the single-polaron optical conductivity. The reduction in intensity of the polaron optical conductivity band can be interpreted as a decrease of the overall electron-phonon coupling strength due to many-body effects. Correspondingly, at high doping levels, the polaron mass m^* , determined by the sum

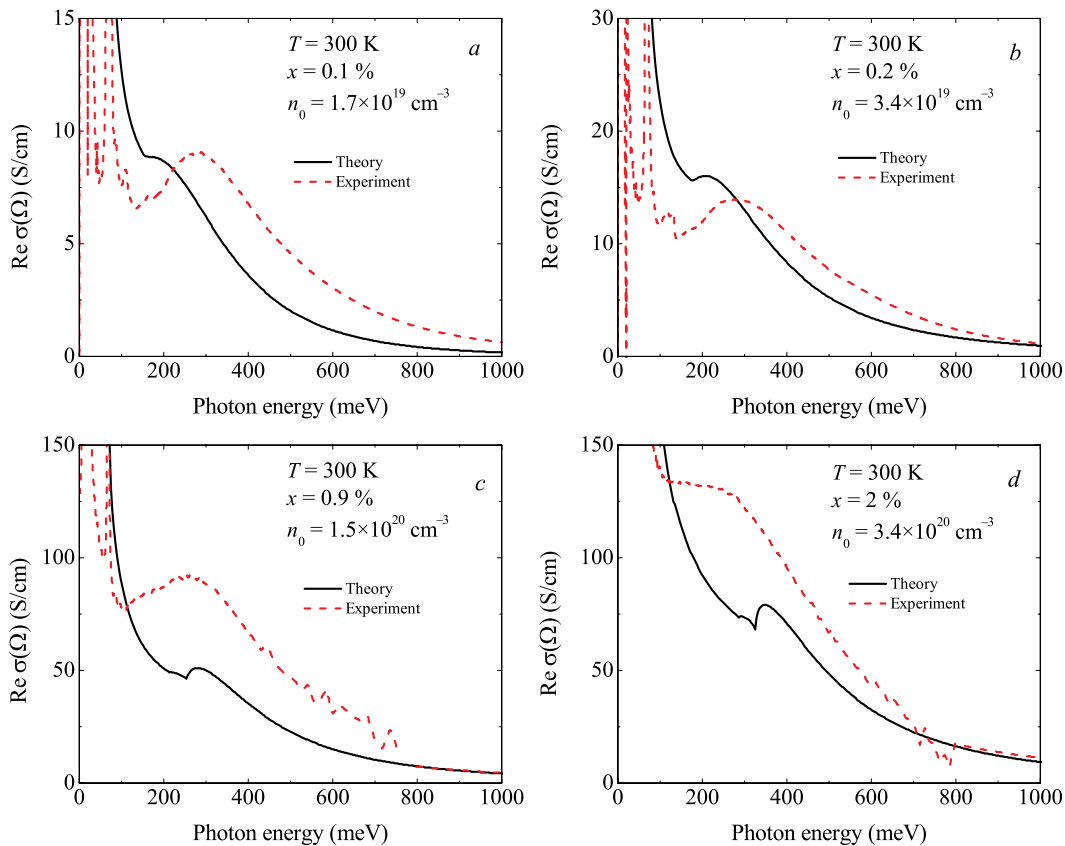


FIG. 3: The many-large-polaron optical conductivity compared with the experiment [17] at $T = 300$ K. The doping level is $x = 0.1\%$ (a), 0.2% (b), 0.9% (c) and 2% (d).

rule introduced in Ref. [53]

$$\frac{\pi e^2 n_0}{2m^*} + \int_{\omega_L}^{\infty} \text{Re}(\Omega) d\Omega = \frac{\pi e^2 n_0}{2\bar{m}_b} \quad (23)$$

is reduced, compared to the single-polaron effective mass. As shown in Refs. [20, 54], the sum rule [53] remains valid for an interacting polaron gas.

The large-polaron theory of the optical absorption based on Ref. [20] explains without any fitting parameters the main characteristics and trends of the observed spectra of Ref. [17] in $\text{SrTi}_{1-x}\text{Nb}_x\text{O}_3$, including doping- and temperature dependence. Nevertheless, some features of the experimental spectra remain to be explained. In particular, at $T = 7$ K, the pronounced peak at $\hbar\Omega \sim 130$ meV in the experimental optical conductivity is not accounted for by the present theoretical analysis. In the theoretical spectra, peaks of much smaller intensity appear at about the same frequency. In the large-polaron theory, those peaks are provided by the interaction between electrons and the LO-phonon branch with energy $\hbar\omega_{L,2} \approx 58.4$ meV, accompanied by the emission of a plasmon as described in Ref. [20].

The intensity of the experimentally observed absorption peak at $\hbar\Omega \sim 130$ meV is considerably higher than described by the large-polaron theory. In the low density limit, the experimental optical data more rapidly

approach the single polaron limit [33] than the theoretical predictions based on Eq. (10). This absorption peak at $\hbar\Omega \sim 130$ meV may be provided by other mechanisms, not controlled in the present study. E. g., electron-phonon interaction with low-frequency non-polar (e. g., acoustic) phonons may contribute to the optical conductivity. The squared modulus $|V_{\mathbf{q}}|^2$, which characterizes the coupling strength, for the deformation electron-phonon interaction is $|V_{\mathbf{q}}|^2 \propto q$ [55], while for the Fröhlich interaction, $|V_{\mathbf{q}}|^2 \propto q^{-2}$. Consequently, for the deformation electron-phonon interaction, the short-wavelength phonons may provide non-negligible contributions to the optical conductivity. Also, at sufficiently large q , Umklapp scattering processes with acoustic phonons can play a role. The treatment of contributions due to acoustic phonons (and other mechanisms) is the subject of the future work. Another possible explanation of the absorption peak at $\hbar\Omega \sim 130$ meV is weakened screening in the corresponding energy range due to dynamical-exchange [56].

IV. CONCLUSIONS

Many-polaron optical conductivity spectra, calculated (based on Ref. [20]) within the large-polaron picture without adjustment of material constants, explain essential characteristics of the experimental optical conductivity [17]. The intensities of the calculated many-polaron optical conductivity spectra and the intensities of the experimental mid-infrared bands of the optical conductivity spectra of $\text{SrTi}_{1-x}\text{Nb}_x\text{O}_3$ (from Ref. [17]) are comparable for all considered values of the doping parameter. The doping dependence of the intensity of the mid-infrared band in the theoretical large-polaron spectra is similar to that of the experimental data of Ref. [17]. In the high-frequency range, the theoretical absorption curves describe well the experimental data (especially at low temperature). A remarkable difference between the present theoretical approach and experiment is manifested on the low frequency side of the mid-infrared range, where the experimental optical conductivity shows a sharp and pronounced peak for $\hbar\Omega \sim 130$ meV at 7 K. Although the theoretical curve also shows a feature around the same frequency, its intensity is clearly underestimated. This peak in the absorption spectrum at $\hbar\Omega \sim 130$ meV remains to be explained. The value of the effective electron-phonon coupling constant obtained in the present work ($\alpha_{eff} \approx 2$) corresponds to the intermediate coupling strength of the large-polaron theory.

The alternative small-polaron and mixed-polaron models for the optical conductivity require several fitting parameters. Furthermore, we find that the mixed-polaron model would need a major adjustment of the overall in-

tensity in order to fit experimental spectra.

Contrary to the case of the large polaron, the small-polaron parameters cannot be extracted from experimental data. Moreover, the small-polaron model, for any realistic choice of parameters, shows a frequency dependence in the high-frequency range which is different from that of the experimental optical conductivity. Both the experimental and the theoretical large-polaron optical conductivity decrease as a power function at high frequencies, while the small-polaron optical conductivity falls down exponentially for sufficiently high Ω .

In summary, the many-body large-polaron model based on the Fröhlich interaction accounts for the essential characteristics (except – interestingly – for the intensity of a prominent peak at $\hbar\Omega \sim 130$ meV, that constitutes an interesting challenge for theory) of the experimental mid-infrared optical conductivity band in $\text{SrTi}_{1-x}\text{Nb}_x\text{O}_3$ without any adjustment of material parameters. The large-polaron model gives then a convincing interpretation of the experimentally observed mid-infrared band of $\text{SrTi}_{1-x}\text{Nb}_x\text{O}_3$.

Acknowledgments

This work was supported by FWO-V projects G.0356.06, G.0370.09N, G.0180.09N, G.0365.08, the WOG WO.035.04N (Belgium), and by the Swiss National Science Foundation under Grant No. 200020-125248 and the National Center of Competence in Research (NCCR) Materials with Novel Electronic Properties–MaNEP.

-
- [*] Also at Technische Universiteit Eindhoven, P. B. 513, 5600 MB Eindhoven, The Netherlands.
- [**] On leave of absence from: Department of Theoretical Physics, State University of Moldova, str. A. Mateevici 60, MD-2009 Kishinev, Republic of Moldova.
- [3] S. Lupi, P. Maselli, M. Capizzi, P. Calvani, P. Giura, and P. Roy, *Phys. Rev. Lett.* **83**, 4852 (1999).
- [4] L. Genzel, A. Wittlin, M. Bayer, M. Cardona, E. Schonherr, and A. Simon, *Phys. Rev. B* **40**, 2170 (1989).
- [5] P. Calvani, M. Capizzi, S. Lupi, P. Maselli, A. Paolone, and P. Roy, *Phys. Rev. B* **53**, 2756 (1996).
- [6] S. Lupi, M. Capizzi, P. Calvani, B. Ruzicka, P. Maselli, P. Dore, and A. Paolone, *Phys. Rev. B* **57**, 1248 (1998).
- [7] J.-G. Zhang, X.-X. Bi, E. McRae, P. C. Ecklund, B. C. Sales, M. Mostoller, *Phys. Rev. B* **43**, 5389 (1991).
- [8] C. C. Homes, B. P. Clayman, J. L. Peng, R. L. Greene, *Phys. Rev. B* **56**, 5525 (1997).
- [9] M. K. Crawford, G. Burns, G. V. Chandrashekar, F. H. Dacol, W. E. Farneth, E. M. McCarron, III, and R. J. Smalley, *Phys. Rev. B* **41**, 8933 (1990).
- [10] J. P. Falck, A. Levy, M. A. Kastner, and R. J. Birgeneau, *Phys. Rev. B* **48**, 4043 (1993).
- [11] H. M. Rønnow, Ch. Renner, G. Aeppli, T. Kimura and Y. Tokura, *Nature* **440**, 1025 (2006).
- [12] Ch. Hartinger, F. Mayr, J. Deisenhofer, A. Loidl and T. Kopp, *Phys. Rev. B* **69** 100403R (2004); Ch. Hartinger, F. Mayr, and A. Loidl, *Phys. Rev. B* **73**, 024408 (2006).
- [13] P. Calvani, M. Capizzi, F. Donato, S. Lupi, P. Maselli, and D. Peschiaroli, *Phys. Rev. B* **47**, 8917 (1993).
- [14] J. F. Schooley, W. R. Hosler, and M. L. Cohen, *Phys. Rev. Lett.* **12**, 474 (1964).
- [15] D. M. Eagles, M. Georgiev and P. C. Petrova, *Phys. Rev. B* **54**, 22 (1996).
- [16] C. Z. Bi, J. Y. Ma, J. Yan, X. Fang, B. R. Zhao, D. Z. Yao and X. G. Qiu, *J. Phys.: Condens. Matter* **18**, 2553 (2006).
- [17] J. L. M. van Mechelen, D. van der Marel, C. Grimaldi, A. B. Kuzmenko, N. P. Armitage, N. Reyren, H. Hagemann, and I. I. Mazin, *Phys. Rev. Lett.* **100**, 226403 (2008).
- [18] F. Gervais, J. L. Servoin, A. Baratoff, J. G. Bednorz and G. Binnig, *Phys. Rev. B* **47**, 8187 (1993).
- [19] C. Ang, Z. Yu, Z. Jing, P. Lunkenheimer and A. Loidl, *Phys. Rev. B* **61**, 3922 (2000).
- [20] J. Tempere and J. T. Devreese, *Phys. Rev. B* **64**, 104504 (2001).
- [21] J. T. Devreese and A. S. Alexandrov, *Rep. Prog. Phys.* **72**, 066501 (2009).
- [22] A. S. Alexandrov and J. T. Devreese, *Advances In Po-*

- laron Physics* (Springer, 2009).
- [23] D. M. Eagles, Phys. Rev. **181**, 1278 (1969).
- [24] D. M. Eagles, J. Phys. C **17**, 637 (1984).
- [25] D. M. Eagles and P. Lalousis, J. Phys. C **17**, 655 (1984).
- [26] D. M. Eagles, in *Physics of Disordered Materials*, edited by D. Adler (Plenum, New York, 1985), p. 357.
- [27] H. Fröhlich, Adv. Phys. **3**, 325 (1954).
- [28] H. G. Reik, Z. Phys. **203**, 346 (1967); in *Polarons in Ionic Crystals and Polar Semiconductors* (North-Holland, Amsterdam, 1972).
- [29] H. P. R. Frederikse, W. R. Thurber and W. R. Hosler, Phys. Rev. **134**, A442 (1964).
- [30] E. Ambler, J. H. Colwell, W. R. Hosler and J. F. Schooley, Phys. Rev. **148**, 280 (1966).
- [31] G. Iadonisi, V. Cataudella, G. De Filippis, and D. Ninno, Europhys. Lett., **41**, 309 (1998).
- [32] D. M. Eagles, R. P. S. M. Lobo, and F. Gervais, Phys. Rev. B **52**, 6440 (1995).
- [33] J. Devreese, J. De Sitter, and M. Goovaerts, Phys. Rev. B **5**, 2367 (1972).
- [34] V. L. Gurevich, I. G. Lang, and Yu. A. Firsov, Sov. Phys. Solid State **4**, 918 (1962).
- [35] J. Devreese, W. Huybrechts, and L. Lemmens, Phys. Status Solidi B **48**, 77 (1971).
- [36] E. Kartheuser, R. Evrard, and J. Devreese Phys. Rev. Lett. **22**, 94-97 (1969).
- [37] D. Emin, Phys. Rev. B **48**, 13691 (1993).
- [38] S. N. Klimin, V. M. Fomin, and J. T. Devreese, *to be published*.
- [39] S. N. Klimin, V. M. Fomin, F. Brosens, and J. T. Devreese, Phys. Rev. B **69**, 235324 (2004).
- [40] G. Verbist, F.M. Peeters, J.T. Devreese, Ferroelectrics **130**, 27 (1992).
- [41] N. Choudhury, E. J. Walter, A. I. Kolesnikov, and C.-K. Loong, Phys. Rev. B **77**, 134111 (2008).
- [42] Y. Toyozawa, in: *Polarons in Ionic Crystals and Polar Semiconductors*, North-Holland, Amsterdam (1972), pp. 1 – 27.
- [43] R. Zheng, T. Taguchi, and M. Matsuura, Phys. Rev. B **66**, 075327 (2002).
- [44] M. Born and K. Huang, *Dynamical Theory of Crystal Lattices* (Clarendon, Oxford, 1954).
- [45] R. P. Feynman, R. W. Hellwarth, C. K. Iddings, and P. M. Platzman, Phys. Rev. **127**, 1004 (1962).
- [46] F. M. Peeters and J. T. Devreese, Phys. Rev. B **28**, 6051 (1983).
- [47] X. Wu, F. M. Peeters, and J. T. Devreese, Phys. Rev. B **34**, 2621 (1986).
- [48] R. P. Feynman, Phys. Rev. **97**, 660 (1955).
- [49] L. F. Lemmens, J. T. Devreese, and F. Brosens, Phys. Stat. Sol. (b) **82**, 439 (1977).
- [50] G. D. Mahan, *Many-Particle Physics*, second edition (Plenum Press, 1990).
- [51] N.E. Phillips, B.B. Triplett, R.D. Clear, H.E. Simon, J.K. Hulm, C.K. Jones and R. Mazelsky, Physica **55**, 571 (1971).
- [52] J.L.M. van Mechelen (*to be published*)
- [53] J. T. Devreese, L. F. Lemmens, and J. Van Royen, Phys. Rev. B **15**, 1212 (1977).
- [54] J. Tempere and J. T. Devreese, Eur. Phys. J. B **20**, 27 (2001).
- [55] F. M. Peeters and J. T. Devreese, Phys. Rev. B **32**, 3515 (1985).
- [56] J. T. Devreese, F. Brosens, and L. F. Lemmens, Phys. Rev. B **21**, 1349 (1980); Phys. Rev. B **21**, 1363 (1980).